[redacted]

Copy 42
RM SL56B03

NACA

RESEARCH MEMORANDUM

for the

U. S. Air Force

FLIGHT INVESTIGATION TO DETERMINE THE EFFECT OF JET EXHAUST ON DRAG, TRIM CHARACTERISTICS, AND AFTERBODY PRESSURES OF A 0.125-SCALE ROCKET MODEL OF THE MCDONNELL F-101A AIRPLANE

By Thomas L. Kennedy

Langley Aeronautical Laboratory
Langley Field, Va.

[redacted]

NATIONAL ADVISORY COMMITTEE
FOR AERONAUTICS

WASHINGTON

FEB 13 1956

NACA RM SL56B03

NATIONAL ADVISORY COMMITTEE FOR AERONAUTICS

RESEARCH MEMORANDUM

for the

U. S. Air Force

FLIGHT INVESTIGATION TO DETERMINE THE EFFECT OF JET EXHAUST ON DRAG, TRIM CHARACTERISTICS, AND AFTERBODY PRESSURES OF A 0.125-SCALE ROCKET MODEL OF THE MCDONNELL F-101A AIRPLANE

By Thomas L. Kennedy

SUMMARY

A flight investigation has been conducted to determine the effect of jet exhaust on the drag, trim characteristics, and afterbody pressures of a 0.125-scale rocket model of the McDonnell F-101A airplane. Power-off data were obtained over a Mach number range of 1.04 to 1.9 and power-on data were obtained at a Mach number of about 1.5. The data indicated that with power-on the change in external drag coefficient was within the data accuracy and there was a decrease in trim angle of attack of 1.27° with a corresponding decrease of 0.07 in lift coefficient. Correspondingly, pressure coefficients on the side and bottom of the fuselage indicated a positive increment near the jet exit. As the distance downstream of the jet exit increased, the increment on the bottom of the fuselage increased, whereas the increments on the side decreased to a negative peak.

INTRODUCTION

At the request of the U. S. Air Force, a series of flight tests of 0.125-scale models of the McDonnell F-101A airplane have been made by the Pilotless Aircraft Research Division of the Langley Aeronautical Laboratory. The purpose of the present investigation was to determine the effect of the engine jet exhaust on the drag and trim characteristics of the configuration.

The McDonnell F-101A is a high-speed long-range fighter bomber powered by two Pratt & Whitney J57 turbojet engines. The engine exits are below and well forward of the all-movable horizontal stabilizer and tail. During a portion of the present flight, two solid-propellant rocket motors were used to simulate the jet exhaust characteristics of the turbojet engines. Investigations of other configurations using the rocket-motor-simulator technique are presented in references 1 and 2. Power-on drag and trim characteristics were obtained at a Mach number of about 1.5 and power-off data were obtained over the Mach number range of 1.04 to 1.9. Static longitudinal stability data were obtained with power on at a Mach number of about 1.5 and power-off data were obtained at Mach numbers of about 1.5 and 1.9. Results of a flight test to determine the longitudinal stability of a model with open inlets are presented in reference 3.

SYMBOLS

A_e	jet exit area, sq in.
$\bar{c}$	mean aerodynamic chord, ft
C_{D_B}	base drag coefficient
C_L	lift coefficient
C_{D_E}	external drag coefficient
C_{L_α}	lift-curve slope
C_p	pressure coefficient, $\frac{(p_l - p)144}{q}$
F	thrust, lb
M	Mach number
M_e	exit Mach number
p	free-stream static pressure, lb/sq in. abs
p_e	jet exit static pressure, lb/sq in. abs
p_l	local static pressure, lb/sq in. abs

q	free-stream dynamic pressure, lb/sq ft
R	Reynolds number
S	wing reference area, sq ft
T	free-stream static temperature, $^{\circ}R$
t	time, sec
α	angle of attack of fuselage reference line (corrected to center of gravity)
γ_e	specific heat ratio at jet exit, c_p/c_v
ΔC_p	incremental change in pressure coefficient due to power-on, $C_{p_{power\text{-}on}} - C_{p_{power\text{-}off}}$

MODEL DESCRIPTION

Airframe

The general configuration of the model tested is shown by the three-view drawing presented in figure 1. Photographs of the model are shown in figure 2. Presented in table I are the physical characteristics of the model.

The model was constructed of steel and aluminum plates with plastic hatches and wooden fairings forming the contoured body lines. The actual airplane has wing root inlets which were faired over in this investigation to facilitate installation of the rocket-motor simulator in the engine ducts. Two pulse rockets were installed forward of the canopy to disturb the model in pitch. The model was otherwise similar to the model tested in reference 3.

Turbojet Simulator

Simulation of jet exhaust was accomplished by use of two solid-propellant rocket motors designed according to the method of reference 4. The simulator shown in figure 3 was installed inside the engine ducts. The ducts terminated external to and under the fuselage. The final angle on the curved boattails of the engine ducts was about 25°. The simulator installation was designed to simulate the Pratt & Whitney J57 engine exhaust characteristics at maximum rated power (sonic exit,

[redacted]

afterburner on) at a Mach number of 1.5 and an altitude of 35,000 feet for a test Mach number of 1.5 and an altitude of 12,000 feet.

The simulator flight-test performance data corrected to an altitude of 35,000 feet and full scale by the method of reference 4 are presented in table II with the J57 design figures for comparison.

INSTRUMENTATION

Continuous-wave Doppler radar was used to measure the velocity of the model, and an NACA modified SCR 584 tracking radar was used to obtain the flight path. Atmospheric data were obtained from a rawinsonde released just prior to launching.

An NACA 10-channel telemeter transmitted continuous signals of free-stream pitot stagnation pressure, simulator chamber pressure, angle-of-attack cone base pressure, longitudinal acceleration, normal acceleration, angle of attack, and one set of manifolded model base pressures. Three channels were switched and these channels transmitted intermittent measurements of nine absolute static pressures (three measurements per channel) at various locations: seven on the afterbody, one on the horizontal stabilizer, and one manifold base pressure. A sketch showing the orifice locations is presented in figure 4.

TESTS

Simulator Ground Tests

Three static firings of the sustainer motor were made, and thrust, chamber pressure, and exit static pressure were measured. These tests were used to show that proper simulation would be achieved; they also served to calibrate the variation of exit-static pressure with chamber pressure. This calibration enabled calculation of thrust in flight.

Flight Test

Flight test of the model was conducted at the Pilotless Aircraft Research Station at Wallops Island, Va. A photograph of the model-booster combination on the launcher is shown in figure 5.

[redacted]

Test conditions for the flight are shown in figures 6, 7, and 8. The flight covered a Mach number range of 1.04 to 1.9 with a corresponding Reynolds number range of 5×10^6 to 16×10^6 based on the mean aerodynamic chord. Power-on data were obtained at a Mach number of about 1.5. The ratio of jet static pressure to free-stream static pressure varied from 3.5 to 4.0 during power-on tests as shown in figure 8.

REDUCTION OF DATA

All coefficients, with the exception of pressure coefficients, are based on the theoretical wing area of 5.75 square feet and shown by the dashed lines in figure 1. Velocity measured from CW Doppler radar agreed with that calculated from the measured pitot stagnation pressure except for a period of about 1 second at simulator burnout. Radar appeared to have momentarily lost the model at this time and consequently the value obtained from the measured pitot stagnation pressure was used.

Calibration of the variation of exit-static pressure with chamber pressure in static tests enabled calculation of the thrust in flight by use of the following equation:

$$F = p_e A_e \left(\gamma_e M_e^2 + 1\right) - pA_e$$

Comparison of the vacuum impulse (the first term of the above equation integrated over the burning time) in the static tests to that in flight indicated a total impulse of approximately 10 percent more in flight. The impulse variation in three static tests was less than 3 percent, thus an adjustment of the flight chamber pressure data was indicated. The measured chamber pressure was proportionally adjusted and the resulting thrust used in conjunction with the accelerometer measurements to determine the power-on drag coefficient. The power-on lift coefficients were also corrected to a zero thrust condition.

Drag and lift coefficients were obtained from the measured longitudinal and normal accelerations, corrected to the center of gravity, for the complete Mach number range of the test. The measured base pressures were used to correct the drag coefficients to zero base drag.

Some longitudinal stability data were obtained at several points during the flight. The model was disturbed in pitch by two pulse rockets just prior to sustainer ignition and burnout. All longitudinal stability data were reduced by the method presented in reference 5.

RESULTS AND DISCUSSION

Trim

The trim conditions for the flight are shown in figure 9. The measured trim angle of attack with respect to the fuselage reference line is presented for both the power-on and power-off portions of the flight. The values of power-on trim-lift coefficient were obtained by correcting the measured-lift coefficients for the thrust component along the lift axis. Power-on produced a decrease in trim angle of attack of approximately 1.1° and a trim-lift coefficient decrease of about 0.06 at a Mach number of about 1.5. With the thrust axis through the center of gravity the model change in trim with power-on would have been slightly greater. The model thrust axis was below the center of gravity producing a pitch-up moment, thus alleviating to some extent the pitch-down effect induced by the jet exhaust. The decrease in trim angle of attack corrected to thrust through the center of gravity was approximately 1.27° with a decrease in trim-lift coefficient of approximately 0.072. During power-on, burning of the propellant caused a gradual shift in the center-of-gravity location. The power-off data preceding simulator firing (higher Mach numbers) are for a center-of-gravity location of 21.2 percent $\bar{c}$, and the power-off data for the rest of the flight are for a center-of-gravity location of 17.8 percent $\bar{c}$. The open inlet model of reference 3 indicates a trim at approximately the same Mach number that would correspond to the power-on trim for this model. Since both models had similar stabilizer settings and center-of-gravity locations, it was thought that the difference was caused by either the inlet fairing on this model or the cold jet issuing from the exits of the reference model.

Drag

The power-off external trim-drag coefficient (total drag less base drag) and the base-drag coefficient are shown as a function of Mach number in figure 10. The drag data for this faired inlet model cannot be directly compared to the drag data of the ducted model of reference 3.

The variation of power-on drag coefficient with time for a power-on lift coefficient of 0.11 is shown in figure 11. The power-off drag coefficient for $C_L = 0.11$ shown for comparison was obtained from several drag polars just previous to simulator firing. The power-off data are corrected to zero base drag and during power-on the base-drag coefficient based on the wing area was negligible. The data indicate that the power-on drag coefficient is equal to or as much as 10 percent less than the power-off drag coefficient. This variation is believed to be due to inaccuracies in the determination of thrust. The average power-on drag is less than power-off, but the increment is within the accuracy of the data.

The drag comparison presented herein is not the difference in the airplane drag power off and power on, but shows the effect of the jet exhaust on the external drag. The power-off total-drag coefficient would be greater by the base-drag coefficient and also would involve a change in inlet drag from a low inlet drag at maximum mass flow to a high inlet drag at zero mass flow.

Pressure Coefficients

Figure 12 presents the jet-off pressure coefficients for the various orifice locations and figure 4 indicates the location of these orifices. The discontinuity and temporary increase in several of the coefficients at a Mach number of about 1.5 is believed to have been caused by intermittent burning of propellant remnants. Orifice number 8 (horizontal stabilizer) is omitted at high Mach numbers due to the fact that this pressure varied with angle of attack and since it was measured intermittently it was impossible to get a complete time history. None of the other pressures appeared to be influenced by changes in angle of attack encountered.

Figure 13 shows the incremental change in pressure coefficient caused by the jet exhaust $\left(\Delta C_p = C_{p_{power\text{-}on}} - C_{p_{power\text{-}off}}\right)$ for the power-on portion of the flight. Measurements prior to power-on were used for $C_{p_{power\text{-}off}}$. In figure 13(a) a general increase in pressure along the bottom of the fuselage is indicated with the most forward orifice showing little change and the most rearward orifice showing the greatest increase.

Pressure coefficients on the side of the fuselage, figure 13(b), indicated that power-on caused an increase near the jet gradually decreasing to a high negative change approximately two jet diameters to the rear of the jet exit. The base annulus pressures were increased considerably but the portion of the annulus inboard showed about 35 percent less increase than the outboard portion of the annulus (fig. 13(c)). This effect is believed to be caused by the influence of the body tailpipe juncture in the vicinity of the base. Power-on produced an approximate change in pressure coefficient $\Delta C_p = 0.11$ for orifice number 8 (horizontal stabilizer) but it is not possible to determine what the change would have been with no angle-of-attack change. The small range of the jet-exit static to free-stream static pressure ratio (fig. 8) encountered in flight precludes the determination of the effect of pressure ratio on any of the data presented; however, it is noted that several of the incremental changes follow the same trend as the pressure ratio.

[redacted]

Stability

In figure 14 the lift-curve-slope variation with Mach number is compared with that of reference 3. Comparison with reference 3 shows that there might have been some reduction in power-off C_{L_α} due to fairing over the inlets but, in general, both power-off and power-on show good agreement with the previous tests. There appears to be a slight increase in lift-curve slope with power-on.

The aerodynamic-center location was obtained at several isolated times during the flight from the period of the oscillation and the lift-curve slope. These data are plotted in figure 15 with the data of reference 3 for comparison. The data in general show good agreement with those of reference 3 but because of the technique used it is felt that the effect of the jet exhaust on the center of pressure should not be interpreted from these data.

CONCLUSIONS

A flight investigation has been made to determine the effect of jet exhaust at a Mach number of 1.5 on the drag and trim of a 0.125-scale rocket model of the McDonnell F-101A airplane with the propulsive jet operating. The following effects were noted when a comparison was made between power-on and power-off data:

1. A decrease in external drag coefficient is indicated; however, the average increment is within the accuracy of the data.

2. The propulsive jet caused a decrease in trim angle of attack of approximately 1.27° and a decrease in trim lift coefficient of 0.07.

3. The pressure coefficient for the base annulus was increased, but the increase was smaller on the portion of the annulus adjacent to the fuselage.

4. Pressure coefficients on the side and bottom of the fuselage indicated a positive increment near the jet exit. As the distance downstream of the jet exit increased, the increment on the bottom of the fuselage increased, whereas the increments on the side decreased to a negative peak.

5. A slight increase in the lift-curve slope of the model was indicated. Other effects on stability are considered to be within the accuracy of the data.

Langley Aeronautical Laboratory,
National Advisory Committee for Aeronautics,
Langley Field, Va., January 24, 1956.

for Thomas L. Kennedy
Aeronautical Research Scientist

Approved: Joseph A. Shortal
Joseph A. Shortal
Chief of Pilotless Aircraft Research Division

mr

REFERENCES

1. Falanga, Ralph A., and Judd, Joseph H.: Flight Investigation of the Effect of Underwing Propulsive Jets on the Lift, Drag, and Longitudinal Stability of a Delta-Wing Configuration at Mach Numbers From 1.23 to 1.62. NACA RM L55I13, 1955.

2. Judd, Joseph H., and Falanga, Ralph A.: Flight Investigation of the Effect of a Propulsive Jet Positioned According to the Transonic Area Rule on the Drag Coefficients of a Single-Engine Delta-Wing Configuration at Mach Numbers From 0.83 to 1.36. NACA RM L56A16, 1956.

3. Hastings, Earl C., Jr., and Mitcham, Grady L.: Flight Determination of the Longitudinal Stability and Control Characteristics of a 0.125-Scale Rocket-Boosted Model of the McDonnell F-101A Airplane at Mach Numbers From 0.82 to 1.84. NACA RM SL55F24, U. S. Air Force, 1955.

4. De Moraes, Carlos A., Hagginbothom, William K., Jr., and Falanga, Ralph A.: Design and Evaluation of a Turbojet Exhaust Simulator, Utilizing a Solid-Propellant Rocket Motor, for Use in Free-Flight Aerodynamic Research Models. NACA RM L54I15, 1954.

5. Gillis, Clarence L., Peck, Robert F., and Vitale, A. James: Preliminary Results From a Free-Flight Investigation at Transonic and Supersonic Speeds of the Longitudinal Stability and Control Characteristics of an Airplane Configuration With a Thin Straight Wing of Aspect Ratio 3. NACA RM L9K25a, 1950.

[redacted]

TABLE I

PHYSICAL CHARACTERISTICS OF THE MODEL

Wing:	
Area (theoretical), sq ft	5.75
Span, ft	4.97
Aspect ratio	4.28
Mean aerodynamic chord, ft	1.28
Taper ratio	0.28
Sweepback of leading edge, deg	41.12
Sweepback of trailing edge, deg	19.42
Incidence angle (with respect to center line of model), deg	1.0
Dihedral angle, deg	0
Root thickness (theoretical), percent chord	6.67
Tip thickness, percent chord	5.71
Horizontal tail:	
Total area, sq ft	1.17
Span, ft	1.97
Aspect ratio	3.30
Mean aerodynamic chord, ft	0.62
Taper ratio	0.46
Sweepback of leading edge, deg	39.80
Sweepback of trailing edge, deg	20.93
Dihedral angle, deg	10.0
Root airfoil section	NACA 65A077 (modified)
Tip airfoil section	NACA 65A006 (modified)
Tail length (25 percent of wing mean aerodynamic chord to 25 percent of tail mean aerodynamic chord), ft	3.69
Incidence, deg	-1.2
Fuselage:	
Length, ft	8.38
Width (maximum), ft	0.96
Height (maximum), ft	0.88
Maximum cross-sectional area, sq ft	0.66
Base area (both engines), sq ft	0.169
Jet exit area (both engines), sq ft	0.125
Vertical tail:	
Area above fuselage, sq ft	1.18
Span, ft	0.94
Mean aerodynamic chord (theoretical), ft	1.46
Aspect ratio (theoretical)	0.66
Sweepback angle at leading edge, deg	52.00
Sweepback angle at trailing edge, deg	16.60
Root airfoil section	NACA 65A007
Tip airfoil section	NACA 65A007
Weight and balance:	
Loaded condition:	
Weight, lb	489.75
Wing loading, lb/sq ft	85.3
Center of gravity, percent $\bar{c}$	21.2
Moment of inertia in pitch about center of gravity, slug-ft^2	53.30
Empty condition:	
Weight, lb	455.81
Wing loading, lb/sq ft	79.3
Center of gravity, percent $\bar{c}$	17.8
Moment of inertia in pitch about center of gravity, slug-ft^2	52.64

TABLE II

COMPARISON BETWEEN PERFORMANCES OF SIMULATOR AND PRATT & WHITNEY J57 TURBOJET ENGINE

[Simulator performance corrected to full scale and altitude of 35,000 feet; all data for one engine]

	Rocket simulator	Turbojet design
Jet stagnation temperature, °F abs	4,000	3,200
Specific heat ratio	1.25	1.27
Ratio of jet stagnation to free-stream static pressure	6.3 to 7.2	7.10
Jet thrust, lb	15,200 to 15,900	15,600
Average jet gross weight flow, lb/sec	120	122
Jet exit area (afterburner condition), sq ft	3.99	3.98

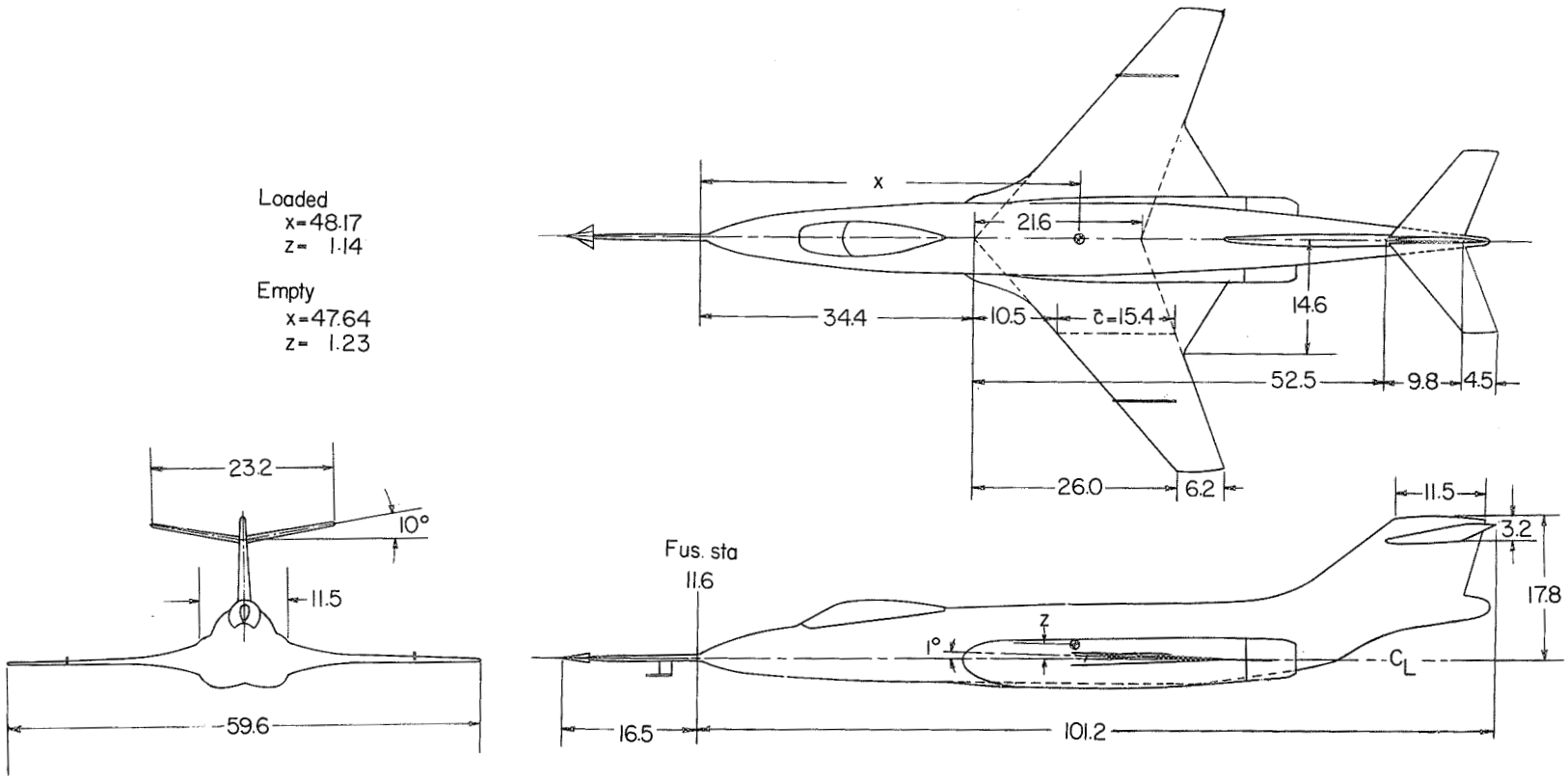

Figure 1.- Three-view drawing of model. All dimensions are in inches.

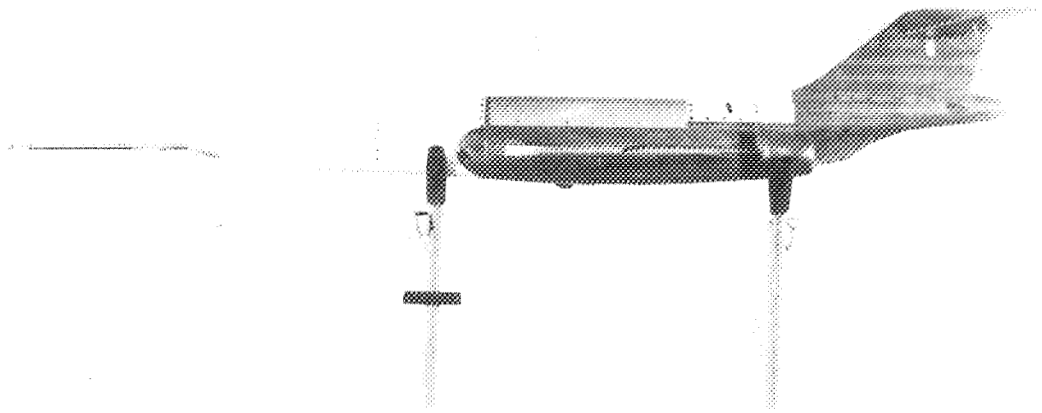

(a) Side view. L-88336.1

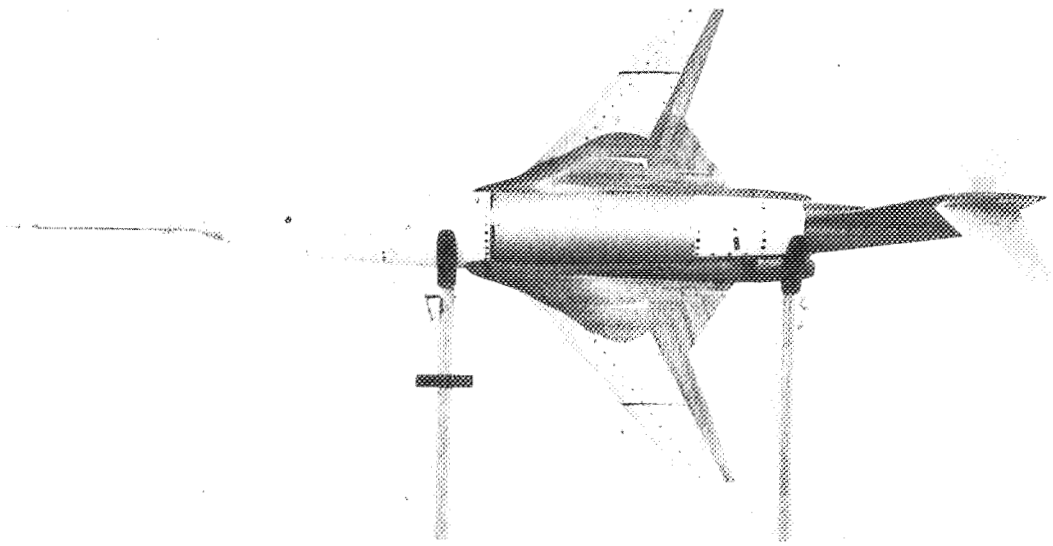

(b) Top view. L-88337.1

Figure 2.- Photograph of model.

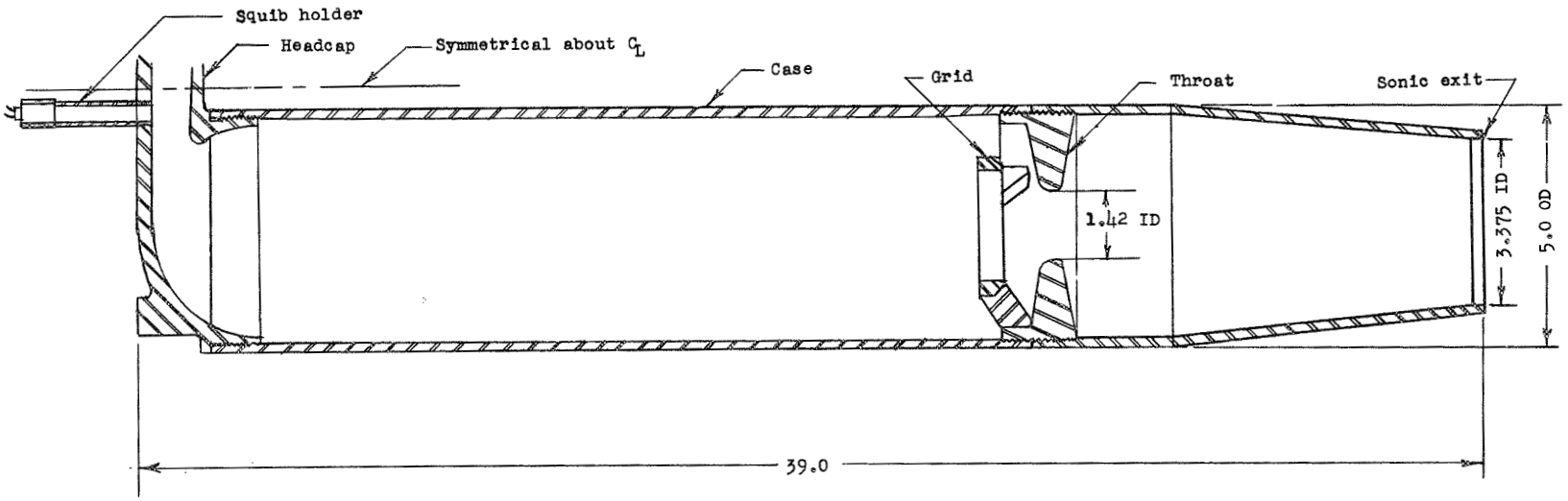

Figure 3.- Sketch of rocket simulator. All dimensions are in inches.

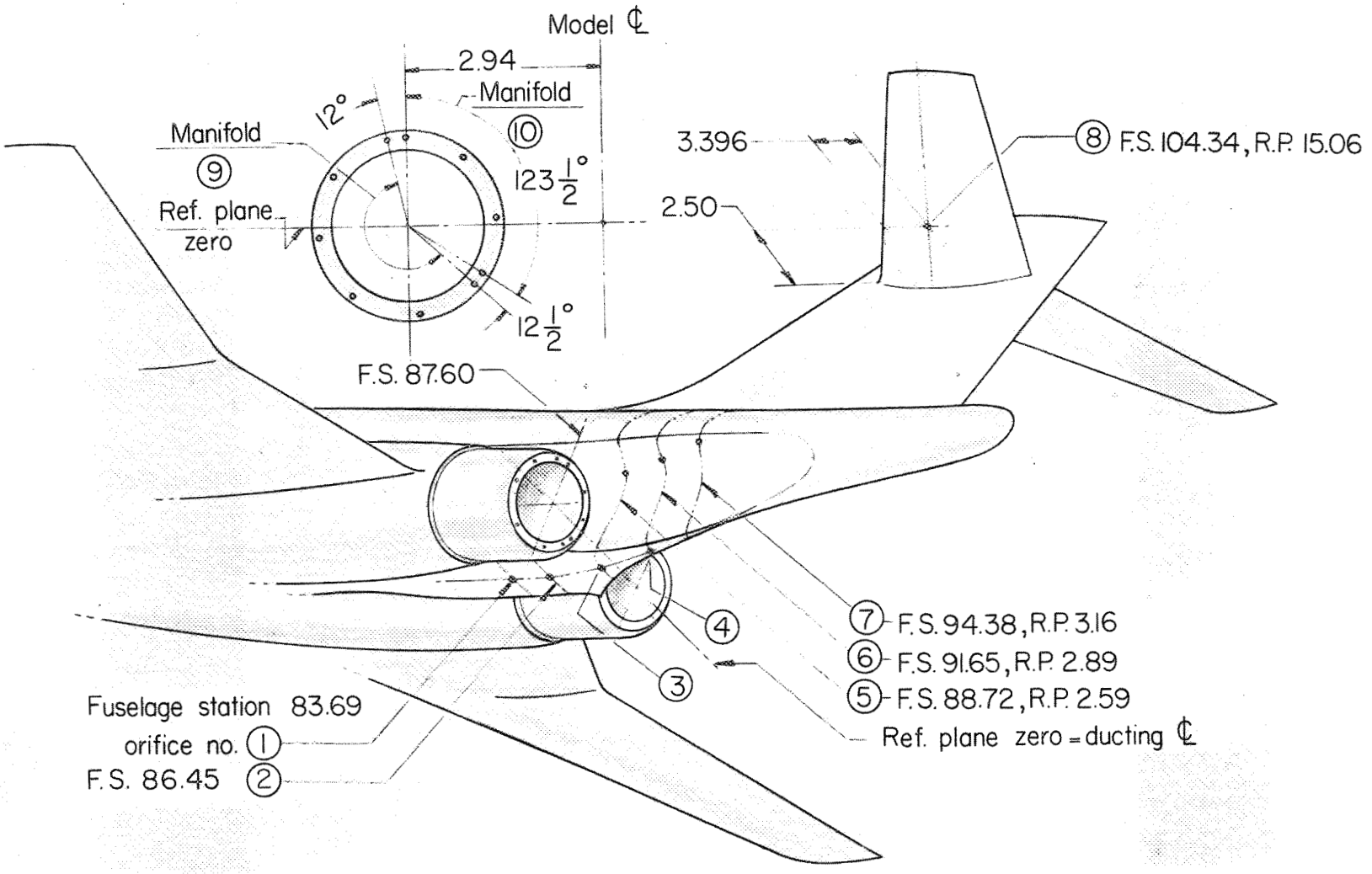

Figure 4.- Pictorial layout of orifice locations.

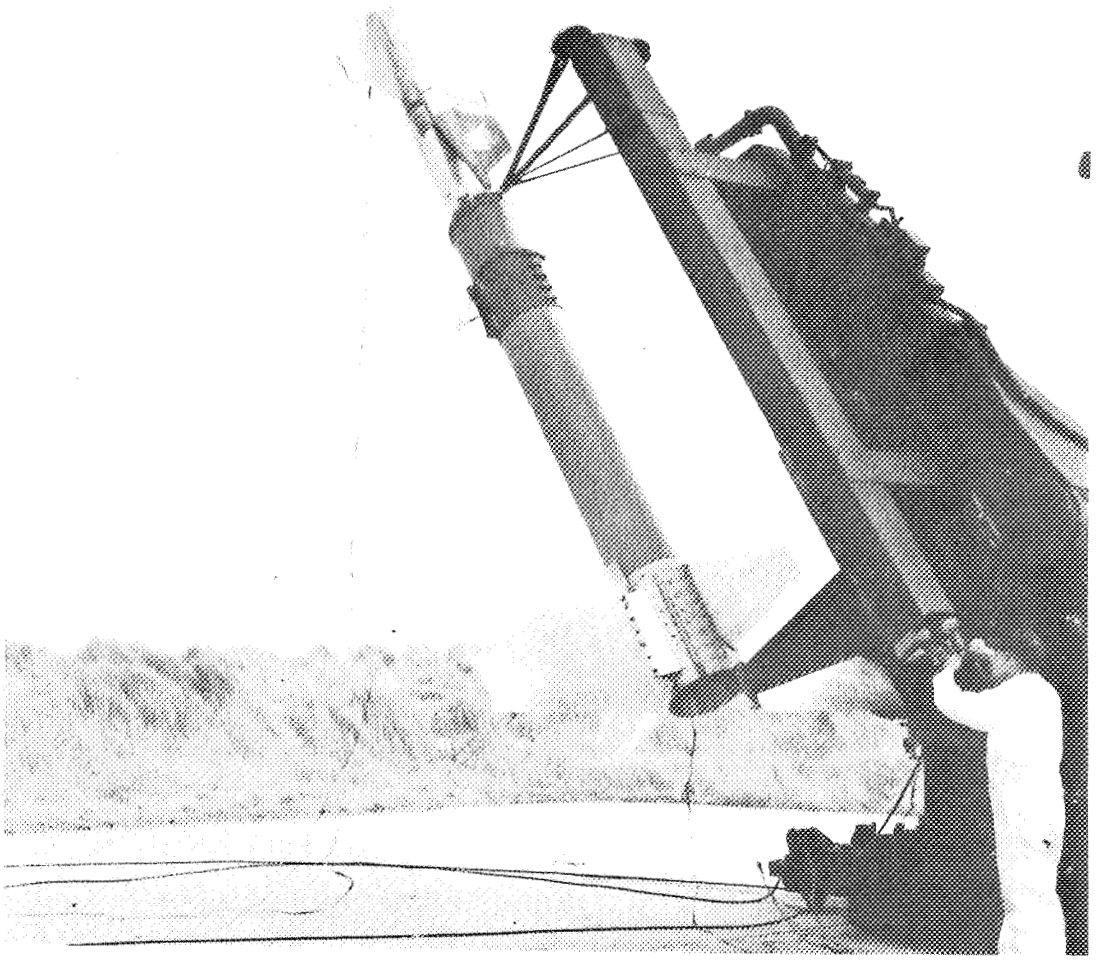

L-88689

Figure 5.- Photograph of model-booster combination on launcher.

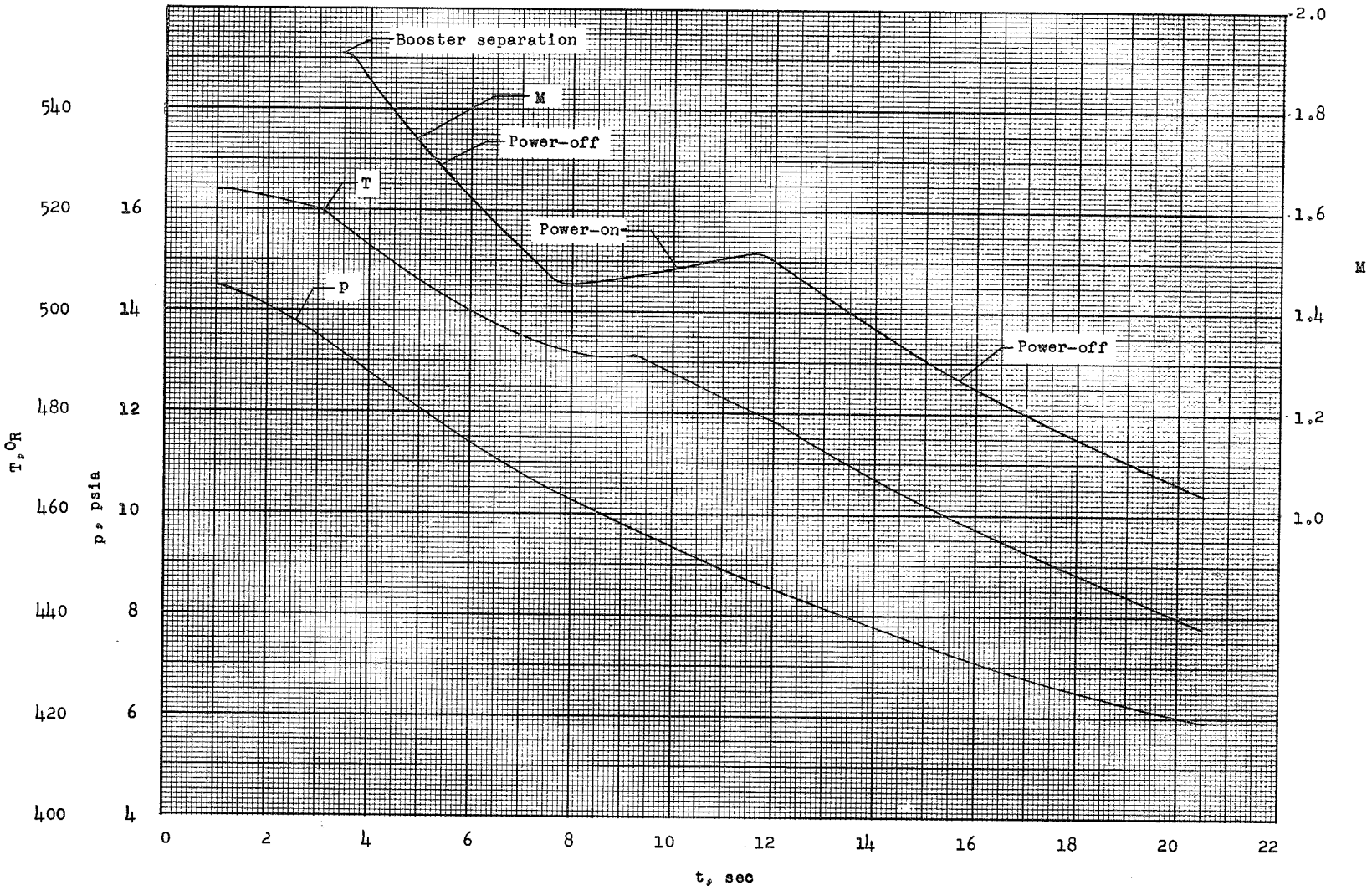

Figure 6.- Static pressure and temperature time history of flight.

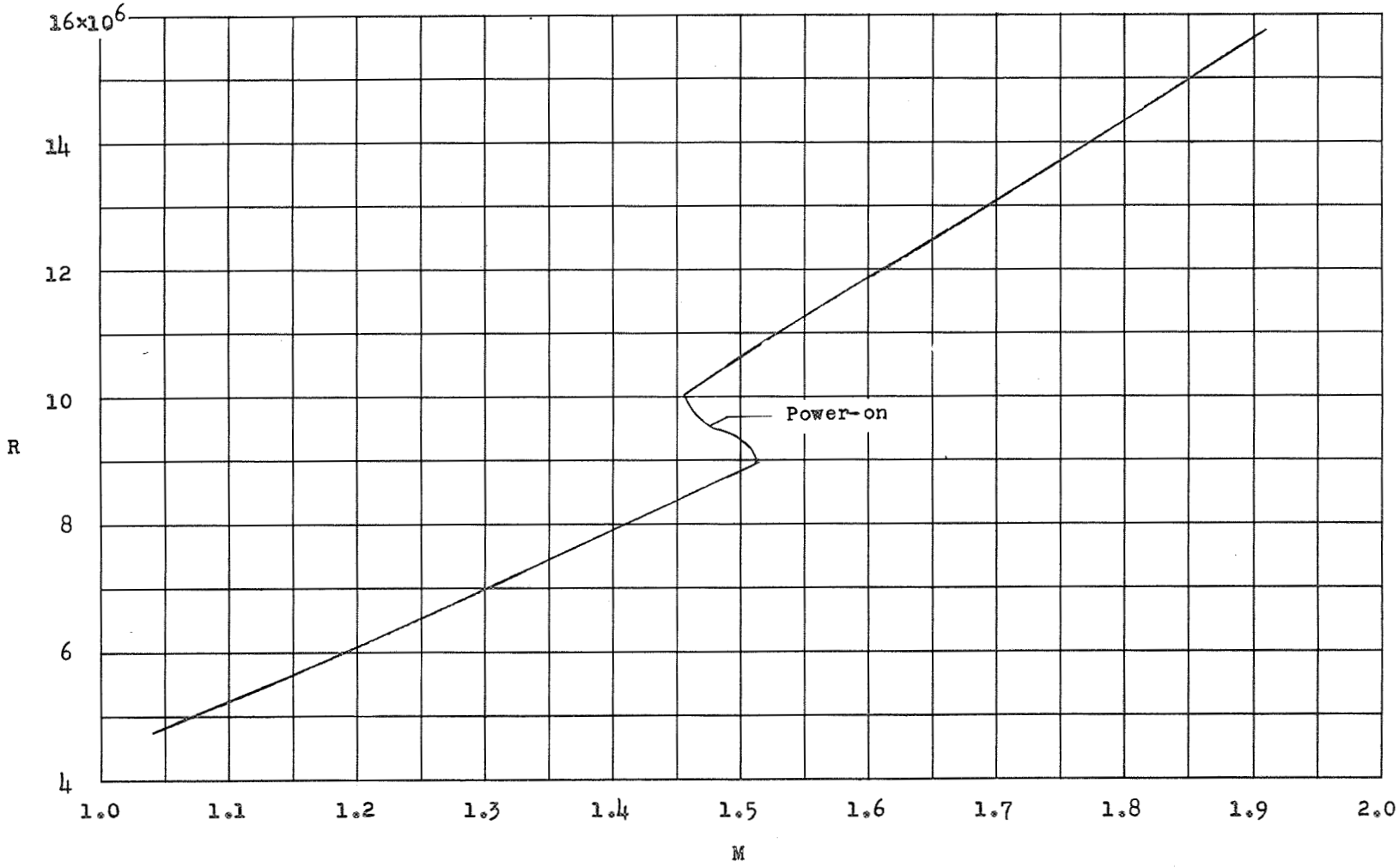

Figure 7.- Reynolds number variation with Mach number.

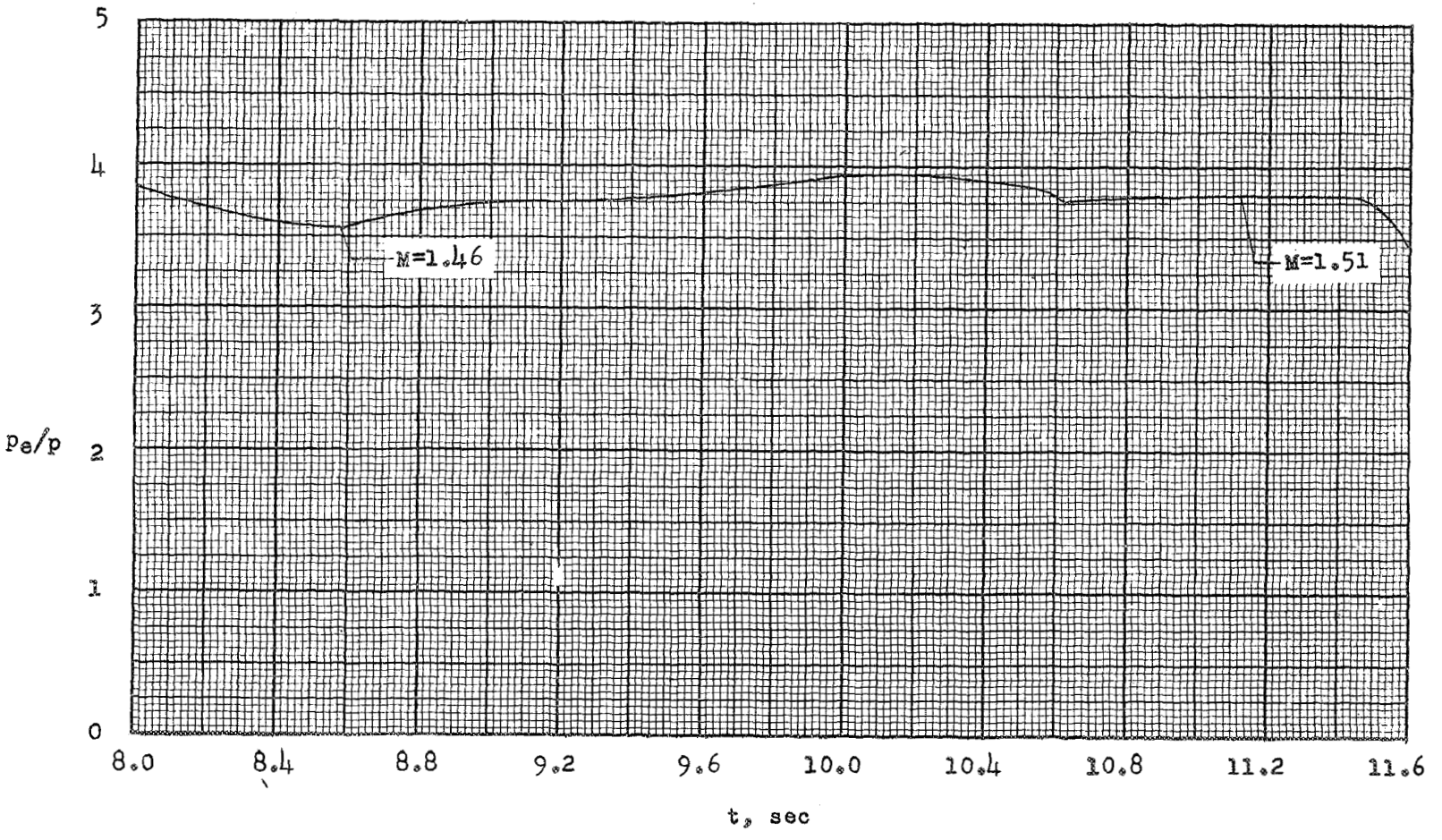

Figure 8.- Variation of ratio of jet-exit static pressure to free-stream static pressure with time for power-on portion of flight.

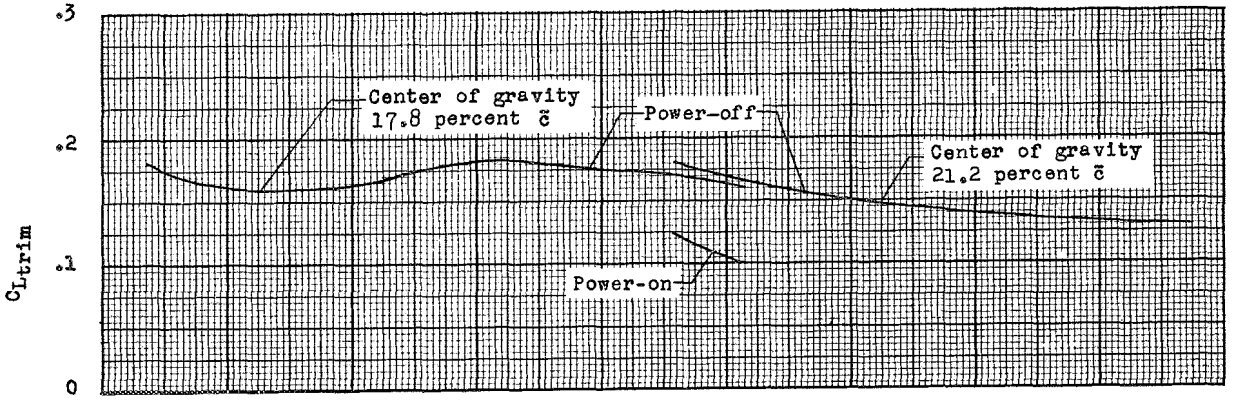

(a) Trim-lift coefficient.

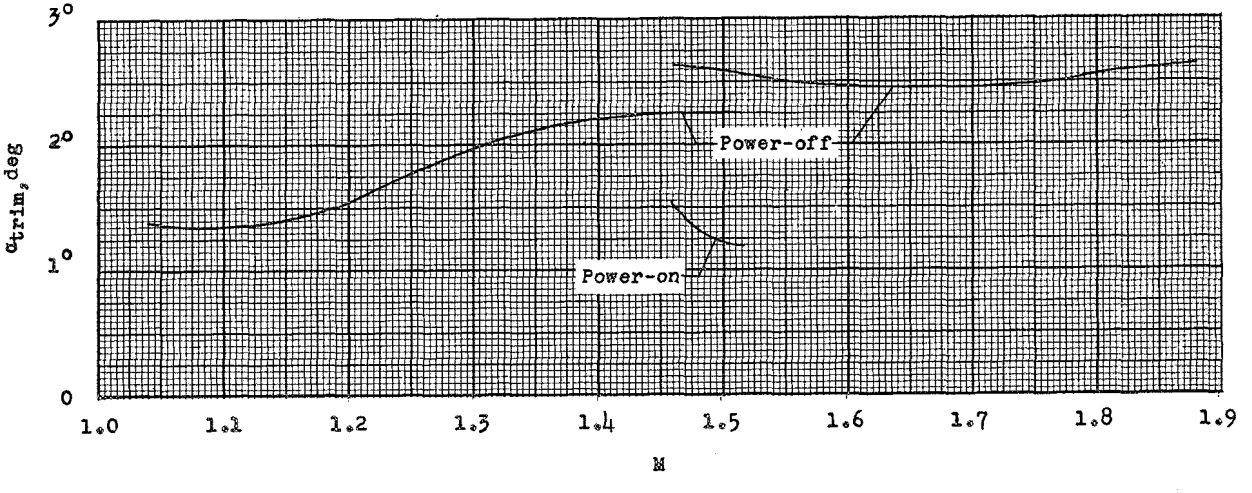

(b) Trim angle of attack.

Figure 9.- Power-on and power-off variation of trim conditions with Mach number.

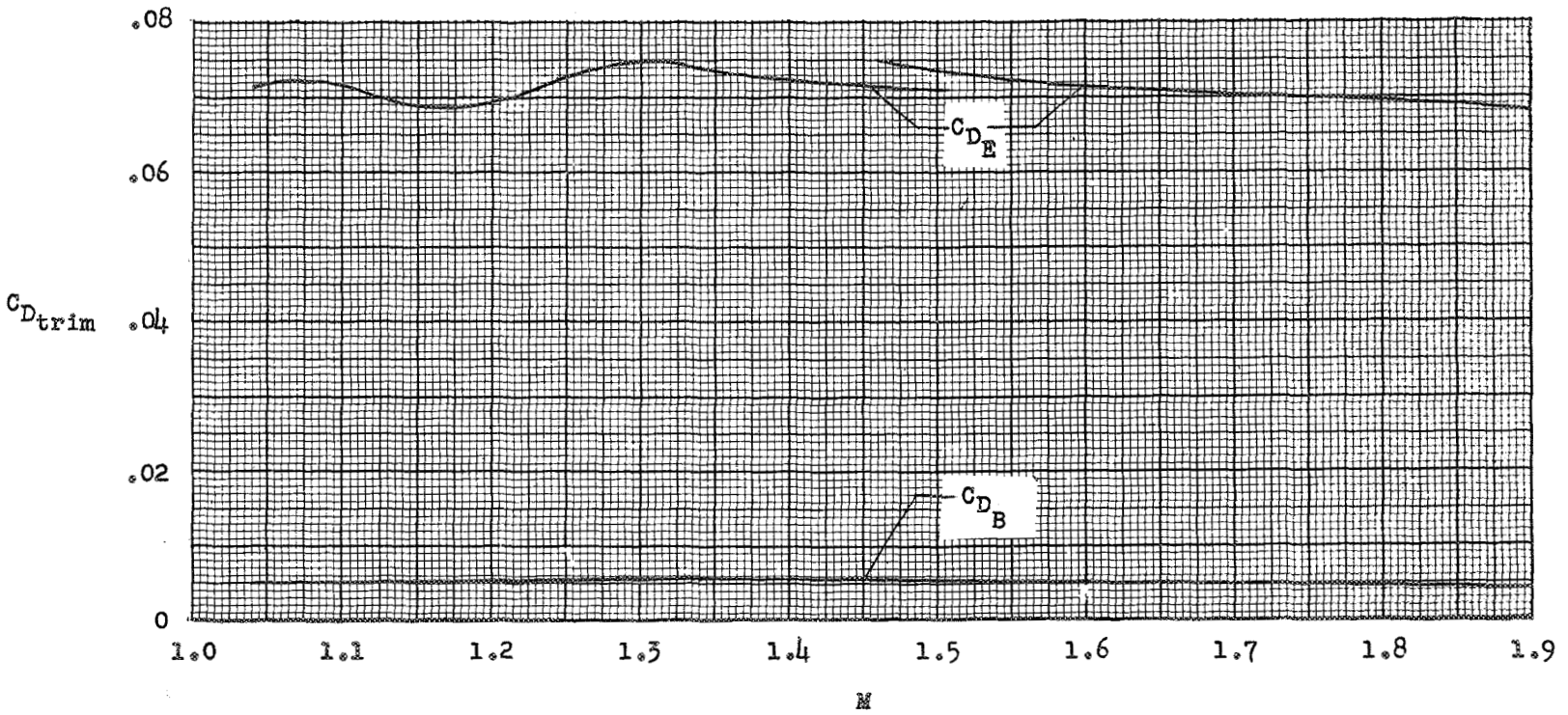

Figure 10.- Variation of power-off trim-drag coefficient with Mach number (based on S = 5.75 sq ft and C_{D_E} corrected to zero base drag).

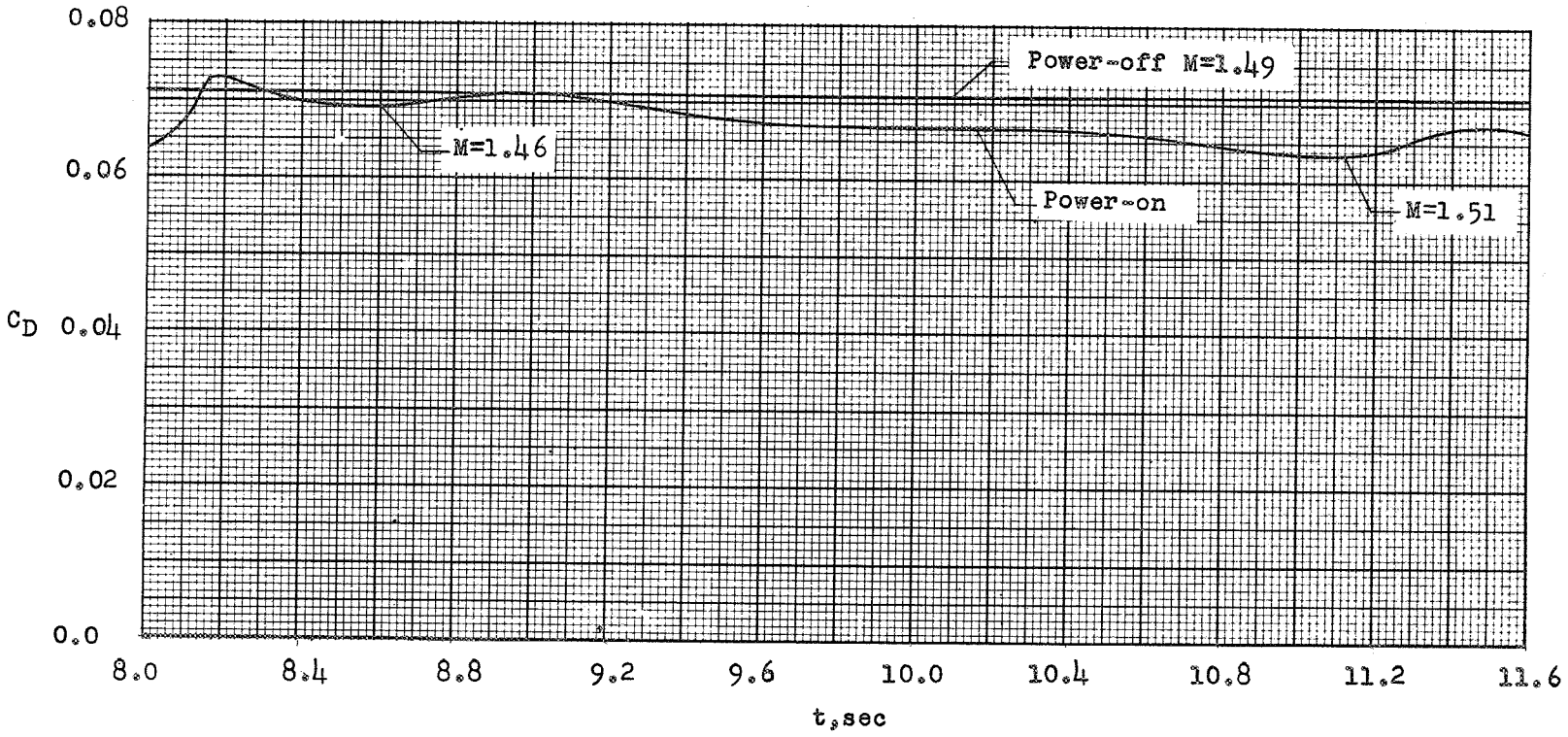

Figure 11.- Variation of power-on drag coefficient with time for lift coefficient of 0.11. C_{D_E} power-off for $C_L = 0.11$ shown for comparison.

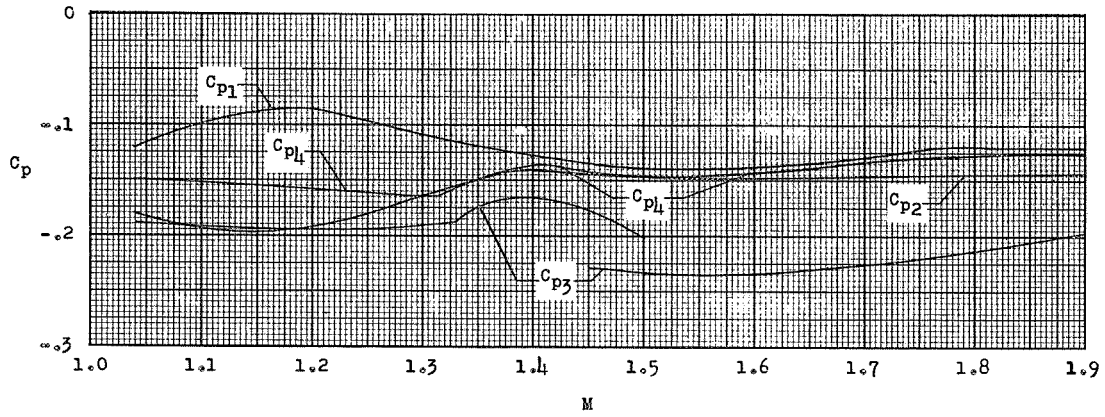

(a) Orifices 1, 2, 3, and 4 (bottom of fuselage).

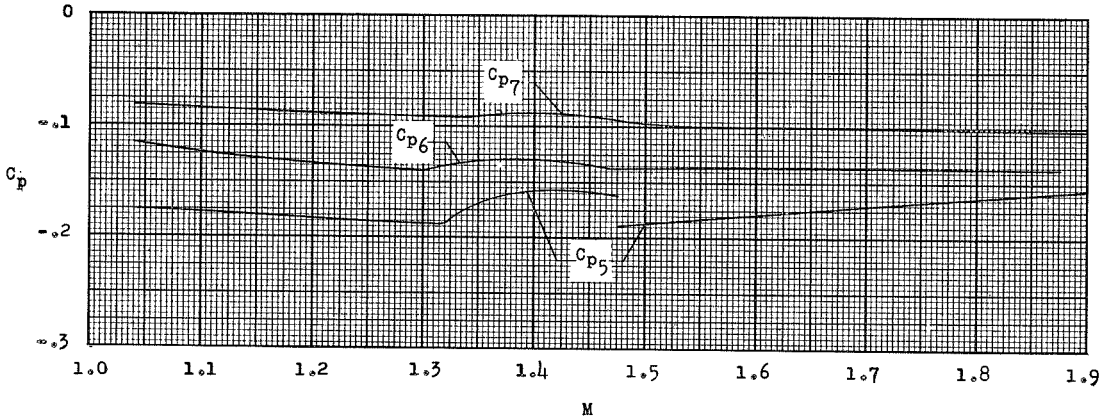

(b) Orifices 5, 6, and 7 (side of fuselage).

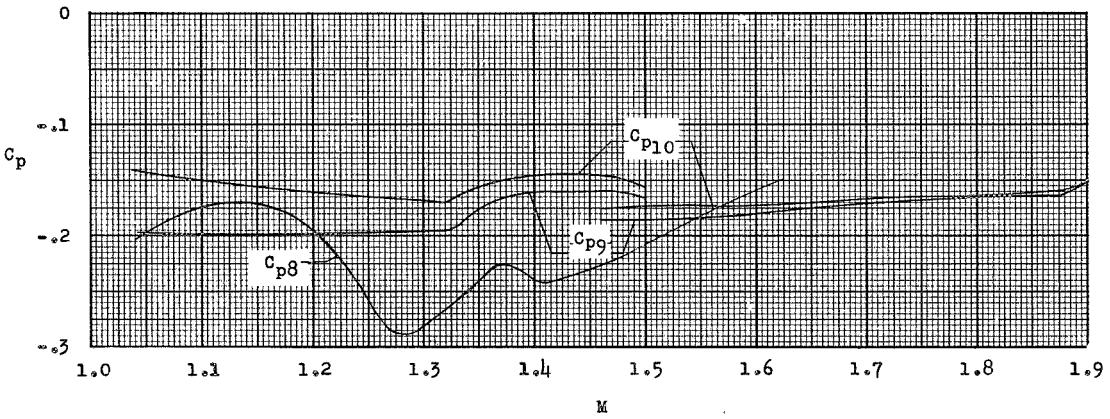

(c) Orifices 8, 9, and 10 (horizontal stabilizer and nacelle base).

Figure 12.- Power-off pressure-coefficient variation with Mach number.

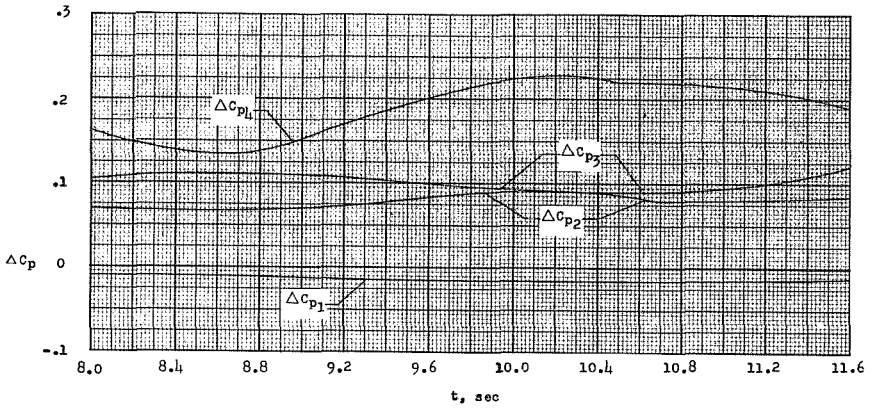

(a) Orifice locations 1, 2, 3, and 4 (bottom of fuselage).

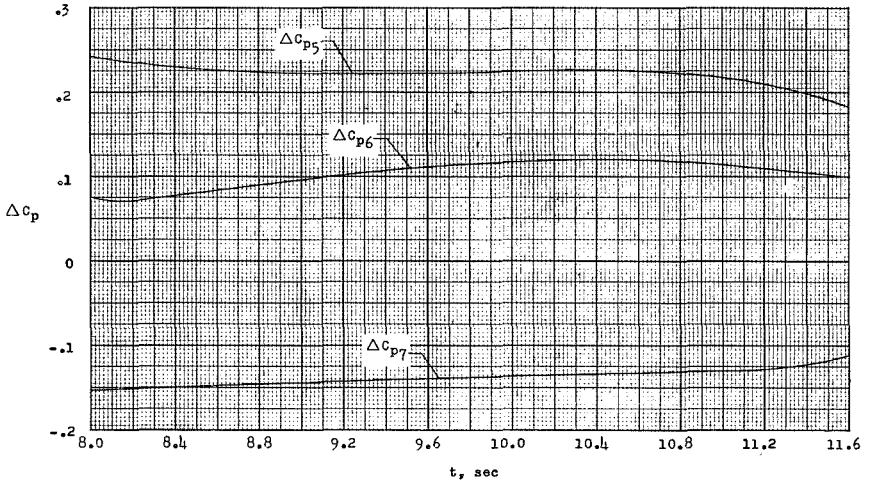

(b) Orifice locations 5, 6, and 7 (side of fuselage).

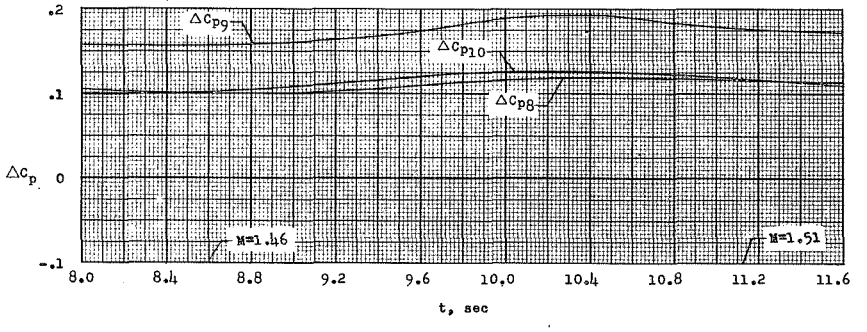

(c) Orifice locations 8, 9, and 10 (horizontal stabilizer and base).

Figure 13.- Variation with time of incremental change in pressure coefficient due to power effects.

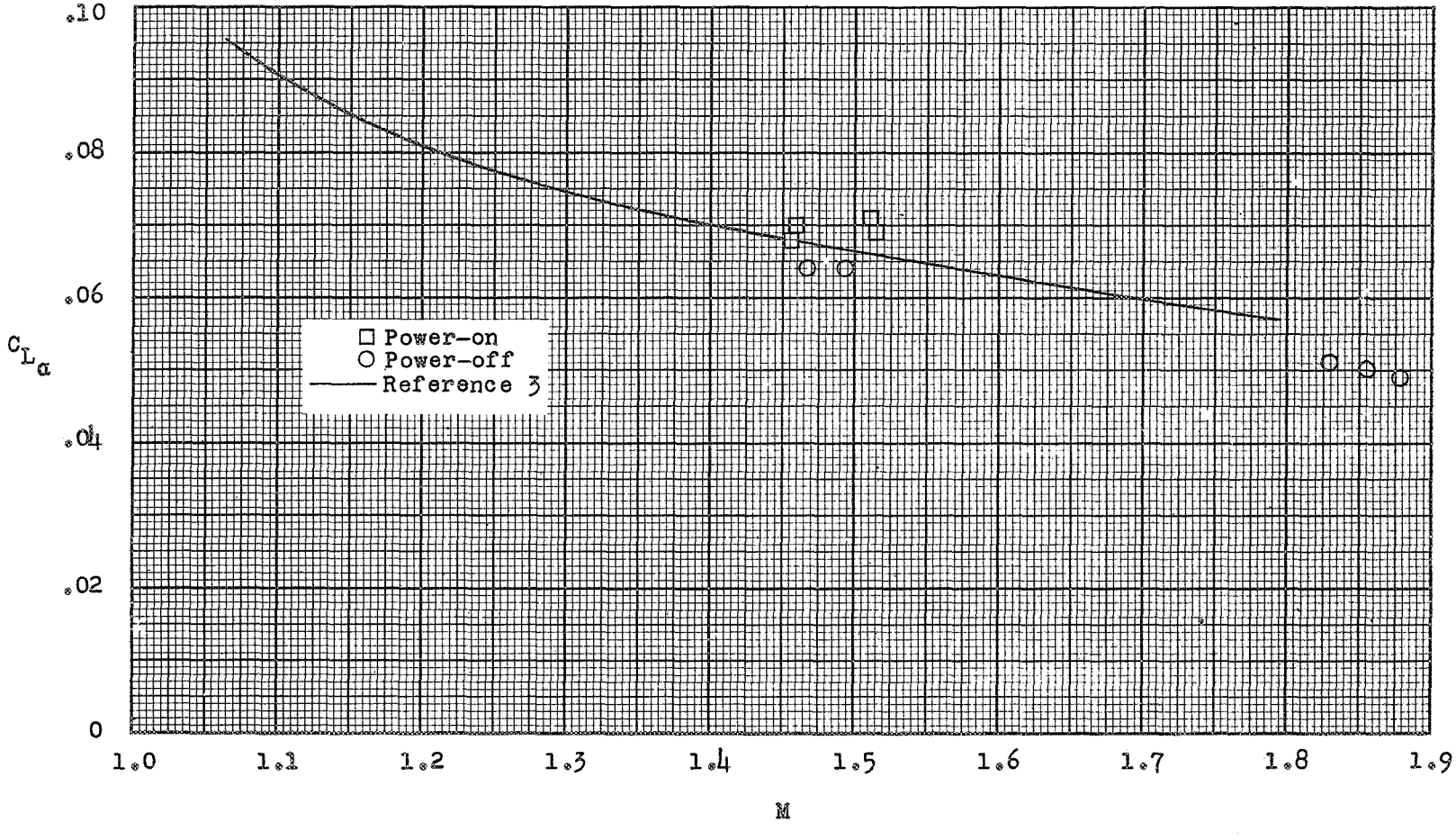

Figure 14.- Variation of lift curve slope with Mach number.

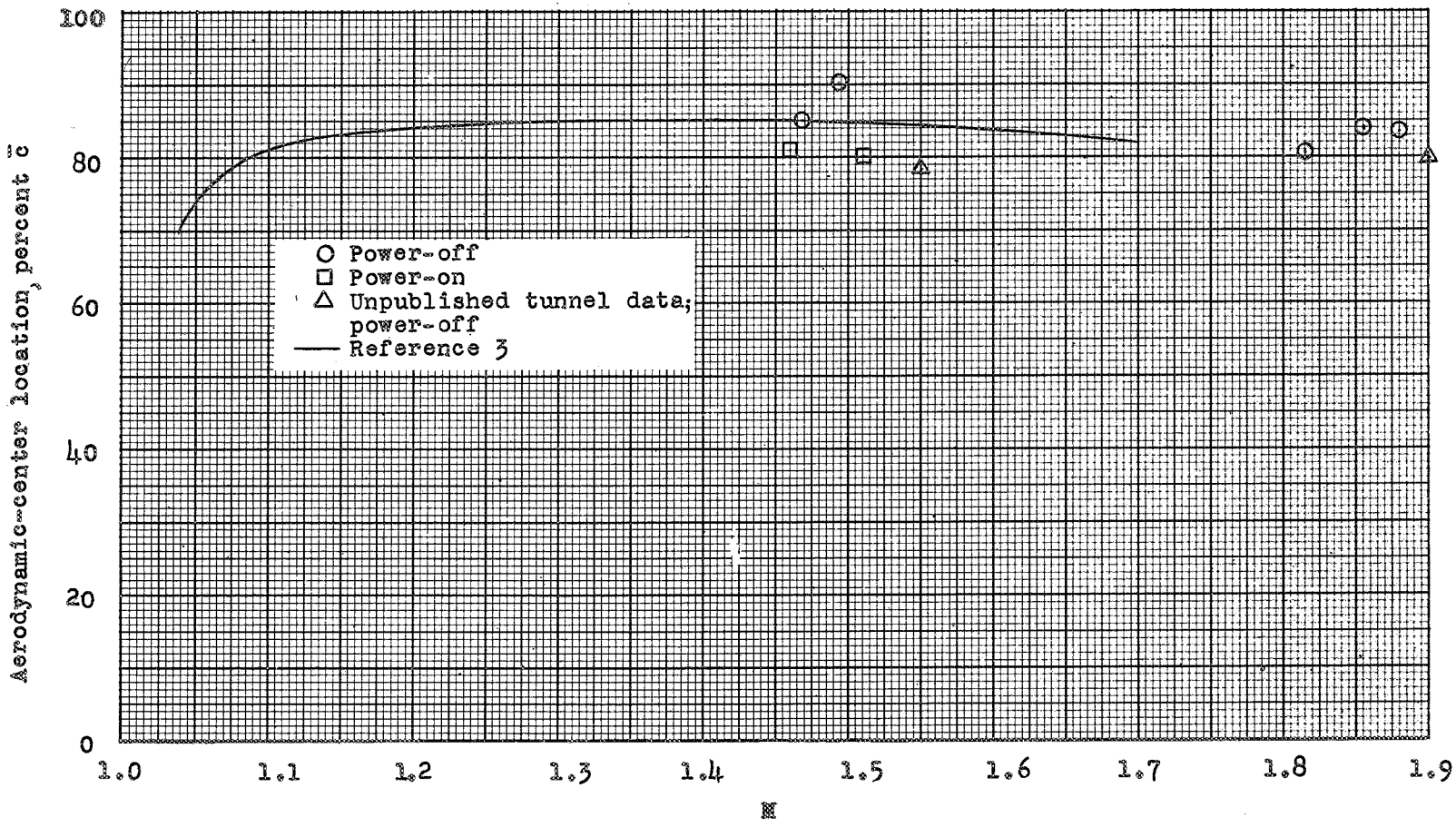

Figure 15.- Aerodynamic-center-of-pressure location. $\bar{c}$ = 1.28 ft.

[redacted]

INDEX

Subject	Number
Exits, Side - Ducted Bodies	1.3.4.4
Exits	1.4.3
Airplanes - Specific Types	1.7.1.2
Stability, Longitudinal - Static	1.8.1.1.1
Loads - Fuselage, Nacelles, and Canopies	4.1.1.3

ABSTRACT

Flight tests of a 0.125 scale model of the McDonnell F101-A airplane were made with a solid propellant rocket motor simulating turbojet with afterburner exhaust at Mach number 1.5. The exhaust jet caused a decrease in trim angle of attack of 1.27° from the jet-off flight condition with a corresponding decrease in trim lift coefficient of 0.07. No measurable change in drag coefficient between jet-on and jet-off flight was noted.

[redacted]